Since January 2020 Elsevier has created a COVID-19 resource centre with free information in English and Mandarin on the novel coronavirus COVID-19. The COVID-19 resource centre is hosted on Elsevier Connect, the company's public news and information website.

Available online at www.sciencedirect.com
SCIENCE DIRECT®
Microbes and Infection 7 (2005) 248–259
Microbes and Infection
www.elsevier.com/locate/micinf

Original article

Microarray and real-time RT-PCR analyses of differential human gene expression patterns induced by severe acute respiratory syndrome (SARS) coronavirus infection of Vero cells

W.F. Leong [a], H.C. Tan [b], E.E. Ooi [b], D.R. Koh [c], Vincent T.K. Chow [a,*]

[a] *Human Genome Laboratory, Department of Microbiology, Faculty of Medicine, National University of Singapore, Kent Ridge, Singapore 117597, Singapore*
[b] *National Environment Agency, Singapore 228231, Singapore*
[c] *Department of Physiology, Faculty of Medicine, National University of Singapore, Kent Ridge, Singapore 117597, Singapore*

Received 21 April 2004; accepted 3 November 2004

Available online 22 January 2005

Abstract

Vero E6 African green monkey kidney cells are highly susceptible to infection with the newly emerging severe acute respiratory syndrome coronavirus (SARS-CoV), and they are permissive for rapid viral replication, with resultant cytopathic effects. We employed cDNA microarray analysis to characterize the cellular transcriptional responses of homologous human genes at 12 h post-infection. Seventy mRNA transcripts belonging to various functional classes exhibited significant alterations in gene expression. There was considerable induction of heat shock proteins that are crucial to the immune response mechanism. Modified levels of several transcripts involved in pro-inflammatory and anti-inflammatory processes exemplified the balance between opposing forces during SARS pathogenesis. Other genes displaying altered transcription included those associated with host translation, cellular metabolism, cell cycle, signal transduction, transcriptional regulation, protein trafficking, protein modulators, and cytoskeletal proteins. Alterations in the levels of several novel transcripts encoding hypothetical proteins and expressed sequence tags were also identified. In addition, transcription of apoptosis-related genes DENN and hIAP1 was upregulated in contrast to FAIM. Elevated Mx1 expression signified a strong host response to mediate antiviral resistance. Also expressed in infected cells was the C-terminal alternative splice variant of the p53 tumor suppressor gene encoding a modified truncated protein that can influence the activity of wild-type p53. We observed the interplay between various mechanisms to favor virus multiplication before full-blown apoptosis and the triggering of several pathways in host cells in an attempt to eliminate the pathogen. Microarray analysis identifies the critical host–pathogen interactions during SARS-CoV infection and provides new insights into the pathophysiology of SARS.

Keywords: Microarray; Real-time RT-PCR; SARS coronavirus; Severe acute respiratory syndrome; Transcriptomics

1. Introduction

In November 2002, a novel infectious agent causing severe acute respiratory syndrome (SARS) emerged in Guangdong province, China. However, a global outbreak alert was declared by the World Health Organization (WHO) only in March 2003. By July 2003, SARS had spread to about 30 nations, resulting in more than 8000 cases with either atypical pneumonia or respiratory distress syndrome. When WHO finally declared the end of the global outbreak in July 2003, SARS had already claimed more than 770 lives. In Singapore alone, there were 238 cases with 205 patients who survived, but 33 fatalities, accounting for a mortality rate of approximately 14%.

During March 2003, a number of laboratories independently reported the isolation of a novel coronavirus (CoV) from SARS patients [1–3]. Thin-section electron microscopy revealed viral particles similar to the morphology of CoV. Sequence analyses demonstrated significant similarity of SARS-CoV to the family Coronaviridae, especially with members belonging to group II CoVs, although the novel CoV was genetically distinct from other known CoVs.

* Corresponding author. Tel.: +65 6874 6200; fax: +65 6776 6872.
E-mail address: micctk@nus.edu.sg (V.T.K. Chow).

1286-4579/$ - see front matter © 2005 Elsevier SAS. All rights reserved.
doi:10.1016/j.micinf.2004.11.004

There have been reports on clinical studies and diagnosis of SARS-CoV-infected patients, on the characterization of SARS-CoV structural [4,5] and nonstructural [6,7] proteins, as well as on vaccines targeting the spike (S) protein [8–10]. Li et al. [11] discovered that angiotensin-converting enzyme 2 (ACE2) binds efficiently to the S1 domain of the SARS-CoV spike protein, thus making it likely to act as the functional receptor for SARS-CoV. This is further corroborated by the observation that transfected NIH-3T3 cells expressing ACE2 can be infected with SARS pseudovirus [12]. Furthermore, human monoclonal antibodies against S1 protein block the ACE2 receptor association, and enable potent neutralization of SARS-CoV [10].

Intriguingly, in stark contrast to the two known human coronaviruses HCoV-299E and HCoV-OC43 which usually cause common cold-like symptoms, SARS-CoV exerts a more devastating clinical effect. Host–virus interactions involve an elaborate interplay between molecular pathways initiated by the host in response to viral replication, counteracted by mechanisms triggered by the virus to favor its propagation. Insights into the host antiviral strategies as well as viral pathogenesis can be achieved through the elucidation of these host- and virus-mediated transcriptional responses, which may provide clues to disease manifestations caused by the virus.

Here we report the application of cDNA microarray analysis of the changes in transcriptional activities of African green monkey (*Cercopithecus aethiops*) kidney clone E6 (Vero E6) cells induced by SARS-CoV infection. Unlike many animal coronaviruses, which infect only cells of their natural host species, SARS-CoV can infect and replicate rapidly in cultured cells of different but related species, such as Vero E6 cells, within a 24-h period [13]. In addition, expression profiles of specific genes, including differentially expressed in normal and neoplastic cells or MAP-kinase activating death domain (DENN/MADD), Fas apoptotic inhibitory molecule (FAIM), inhibitor of apoptosis protein 1 (hIAP1) and myxovirus (influenza virus) resistance 1 (Mx1), were analyzed. We also investigated expression of the p53 tumor suppressor gene and its alternative splice variant in SARS-CoV-infected cells. These genes play important roles in apoptosis and in host antiviral resistance. Our study can serve as a basis for more detailed investigations into the exact roles of critical genes and pathways in the pathogenesis of this newly emerging lethal infectious disease of humans.

2. Materials and methods

2.1. Cell culture and virus infection

Vero E6 cells (ATCC number CRL-1586) were cultured in M199 medium (Invitrogen, Carlsbad, CA) supplemented with 10% fetal calf serum, 2.2 g l^{-1} sodium bicarbonate, 10 mM HEPES, 0.1 mM non-essential amino acids, 1 mM sodium pyruvate at 37 °C under 5% CO_2 in a humidified incubator. When cells reached ~90% confluency, one batch of Vero E6 cells that served as the control was mock infected with sterile medium [14,15]. Another batch was infected with SARS-CoV (2003VA2774 isolated from a SARS patient in Singapore) at a multiplicity of infection (MOI) of 1 [13], with a virus inoculum volume of 0.75 ml diluted with 1.25 ml of maintenance medium with only 3% fetal calf serum. After adsorption for 1 h, the inoculum was removed, and 20 ml of maintenance medium was added. At 12 h post-infection, cytopathic effects (CPE) were observed in infected cells. Following incubation at 37 °C for 12 h, both uninfected and infected Vero E6 cells were harvested for RNA extraction. This protocol was designed to minimize any effects on gene expression from "carry-over" cytokines or chemokines in the cell culture supernatant. Moreover, Vero cells are deficient in the interferon (IFN)-alpha/beta response [16]. Viral culture and RNA isolation were carried out in a biosafety level 3 laboratory.

2.2. Total RNA preparation

Total cellular RNA was extracted from uninfected and SARS-CoV-infected Vero E6 cells using an RNeasy Mini Total RNA extraction kit (Qiagen, Hilden, Germany). The RNA was suspended in nuclease-free water, and the concentration quantitated by UV spectrophotometry at 260 nm. The integrity of the extracted RNA was confirmed by electrophoresis in a 1% denaturing agarose gel.

2.3. Microarray hybridization and analysis

Total RNA (25 μg) extracted from each batch of uninfected and SARS-CoV-infected Vero E6 cells was reverse transcribed and labeled with Cy3- and Cy5-dCTP, respectively, using a CyScribe first-strand cDNA labeling kit (Amersham Biosciences, Piscataway, NJ) with anchored oligo(dT) and random nonamers. Labeled cDNAs were purified using a CyScribe GFX purification kit (Amersham Biosciences) and resuspended in 60 μl of elution buffer. The amounts of Cy3- and Cy5-labeled cDNAs were measured at absorbances of 550 and 650 nm, respectively, and calculated based on the following formula: (absorbance/extinction coefficient) × volume of cDNA × dilution factor × 10^{12}. The extinction coefficients for Cy3 and Cy5 were 150,000 and 250,000 l mol^{-1} cm^{-1}, respectively.

The experiments were performed using the IntelliGene II Human 16K cDNA microarray set (Takara Bio, Shiga, Japan), which comprises a total of 16,000 human genes spotted onto four slides, each consisting of 4000 genes. This cDNA-based array consists of ~200–1000-bp fragments representing a wide range of known genes, hypothetical genes and expressed sequence tags (ESTs).

The Cy3- and Cy5-labeled cDNA samples (40 pmol each) were hybridized to each microarray slide at 40 °C for 17 h within a Lucidea SlidePro hybridization chamber (Amersham Biosciences). The slides were washed according to the manufacturer's recommendations. Each slide was scanned

with the GenePix 4000B image scanner, and the data were collected with the GenePix Pro 4.1 software (Axon Instruments, Union City, CA). The raw data were analyzed using Acuity software version 3.1 (Axon Instruments), as well as MIDAS software version 2.17, available at the TIGR website (http://www.tigr.org/software/tm4/) [17]. The typical flow of the MIDAS involved the low-intensity filter, LOWESS normalization, standard deviation regularization, and SLICE analysis [18].

2.4. cDNA synthesis and real-time SYBR Green RT-PCR detection

Total RNA (4 μg) was reverse transcribed in a 40-μl reaction mix containing 1 × first-strand buffer, 10 mM dithiothreitol, 600 ng random hexamers, 0.5 mM deoxyribonucleoside triphosphates, 10 U RNase inhibitor and 200 U SuperScript reverse transcriptase (Invitrogen). Synthesized cDNA was aliquoted and stored at –80 °C.

The differential expression of 17 genes selected after the microarray analysis was further validated by real-time quantitative RT-PCR using SYBR Green-based detection with a LightCycler system (Roche, Basel, Switzerland). In addition, the expression profiles of DENN, FAIM, hIAP1 and Mx1 genes were included in the real-time RT-PCR analysis. All the primers were designed based on the corresponding human mRNA sequences (Table 1). SARS-CoV RNA was also amplified using the primers described by Peiris et al. [2]. Each 10-μl reaction included 1–2 μl of cDNA, 0.5 μM of each primer, 2.5–3 mM $MgCl_2$, and 1 μl of ready-to-use 10 × Hot Start reaction mix (Roche). The reactions were subjected to an initial denaturation of 95 °C for 10 min, followed by 40 cycles each of 95 °C for 10 s, 58–68 °C for 5 s and 72 °C for 10 s, before being subjected to melting curve analysis. Amplified products were also analyzed for specificity by agarose gel electrophoresis, and were further verified by automated cycle sequencing. The conserved HUEL gene was selected as the housekeeping gene transcript to normalize the samples, as its expression level was previously confirmed to be reliably constant in a number of representative tissues [19,20]. To ensure consistency in threshold cycle (C_T) values, duplicate reactions were performed (i.e. from each of the two cDNA preparations of each RNA sample), and the mean C_T values were used for calculating the relative expression levels. The C_T values were analyzed as described previously [21,22], and the normalized C_T values of each gene were subjected to Student's *t*-test with two-tailed distribution to determine the significance at the 95% confidence level.

2.5. Classical RT-PCR amplification of p53 splice variant

Each cDNA sample was subjected to classical RT-PCR amplification of the p53 splice variant using primers P53U and P53D spanning exons 7–10, and the products were electrophoresed in an agarose gel [23]. The target cDNA fragment size of the alternative p53 transcript was expected to be 133 bp larger than the wild-type p53 transcript. Amplified fragments were cloned into pGEM T-Easy vector (Promega, Madison, WI) and directly sequenced.

Table 1
Sequences of primers for the amplification of selected genes evaluated by real-time RT-PCR

Gene	Primer sequence (5′ → 3′)		Target size (bp)
	Sense	Antisense	
ANXA2	GTGACTTCCGCAAGCTGATG	CTGAATGCACTGAACCAGGT	299
CLK1	CCAACCATGTGATGTCTGGA	AGGTCAAAGAGACGCTCATG	288
CTSL	AGGCAGGTGATGAATGGCTT	ACCATTGCAGCCTTCATTGC	276
DENN[a]	GCTAGTGGATCTGGACAG	CATCCACAGAATCCACATCG	275
DUSP1	AGCAGAGGCGAAGCATCATC	GGATGTGAAGAGCCTCACCT	270
EEF1G	TCAGACCTTCATGAGCTGCA	TACTCTCGAACCAGCGTCTG	249
FAIM[a]	ACTACATCAGGCAAACGAGT	GCACCATACGTCCATAGCAT	294
HAVCR1	ACCATGAACCAGTAGCCACT	GCAAGAAGCACCAAGACAGA	265
hIAP1[a]	CAGAAGACACAGACGTCTTTA	CGAACTGTACCCTTGATTGTA	350
HSPA1A	AAGCAGACGCAGATCTTCAC	CTCGATCTCCTCCTTGCTCA	282
HSPCA	GGCAGAGGCTGATAAGAACG	TCTTCCATGCGTGATGTGTC	243
HUEL[b]	TCAGACGACGAAGTCCCCATGAAG	TCCTTACGCAATTTTTTCTCTCTGGC	130
IGFBP3	ACAGCATGCAGAGCAAGTAGAC	CTGCTCTTTGCTGACTACTGGA	245
IL8RA	CTAATTAGCATGGCCACATCT	CAGACACTGCAACACACCTGA	220
KLF5	CCACCTGTACCAGCTACTGA	CTGGAGCATCTCTGCTTGTC	283
MADH2	GCTCTTCTGGCTCAGTCTGT	TAGGGACCACACACAATGCT	305
Mx1[a]	GCCAGGACCAGGTATACAG	GCCTGCGTCAGCCGTGC	361
NFKB1A	ACCTGGTGTCACTCCTGTTG	AGCTCGTCCTCTGTGAACTC	217
NPC2	AGCTCTGCTGCTTCAACAAC	AGGTGTAGAAAGAGGCCACA	223
RAC1	CTGACCAGCTTTTGCGGAGA	AGGCATGGCAGGTGTAAGAG	289
SARS-CoV[a]	TACACACCTCAGCGTTG	CACGAACGTGACGAAT	182
STAM1	TGGTCAGTTCCGTTCAAGGA	TAGCAGGTATCTGCCACCAA	268
TIMP2	AAGCGGTCAGTGAGAAGGAA	GGCACGATGAAGTCACAGAG	253

[a] Genes included for real-time RT-PCR in addition to those selected from the microarray analysis.
[b] Housekeeping gene transcript serving as the normalization control for real-time RT-PCR.

3. Results

3.1. Microarray analysis of SARS-CoV-induced CPE of Vero E6 cells reveals novel differential human gene expression profiles

By 12 h post-infection, ~50% of the cell population is infected, ~25% of the cells round off, with resultant production of an enormous number of virus particles, indicating the suitability of using Vero E6 as host cells for SARS-CoV infection [13].

The slides were scanned for Cy3 and Cy5 signals with a dual-color image scanner. The majority of signals were of relatively low intensity, which could likely be due to the hybridization of primate cDNAs against a human gene-based microarray. However, a significant number of spots displayed strong intensities, thus facilitating the analysis. The latter spots represent highly conserved primate cDNAs, as evidenced by the sequence homologies of greater than 95% between primate and human cDNAs of most of the genes analyzed. Stringency was exercised by flagging individual spots of poor quality (e.g. extreme unevenness in signals and streaks), which were omitted from Acuity and MIDAS software analyses. Under the statistical analysis program, we initially conducted a low-intensity filtering based on 30% of the standard deviation of the total background intensity following MIDAS software analysis. We selected this criterion as it allowed us to effectively disregard the low-intensity spots while retaining those of sufficient quality to be analyzed. The filtered data were normalized against the Cy3-labeled uninfected Vero E6 cellular cDNAs as the reference by using locally weighted linear regression (LOWESS) analysis, proposed as a method to remove intensity-dependent effects commonly found in $\log_2$(ratio) values [24]. We employed $\log_2$(ratio) rather than $\log_{10}$(ratio) due to the former's rationality of treating all regulated genes in a similar fashion, and due to the generation of a continuous spectrum of values. The next step was to regularize the standard deviations of the normalized data to adjust for the variance of the measured $\log_2$(ratio) values to be similar throughout the entire array, thereby minimizing the variability of the results. Finally, through SLICE analysis, we defined an intensity-dependent Z-score threshold to be greater than 1.96 (i.e. equivalent to those more than 1.96 standard deviations from the local mean), which permitted us to identify 70 genes that were differentially expressed at the 95% confidence level. Of these, 29 transcripts exhibited an increase, while 41 demonstrated a decrease in expression level greater than fourfold, based on MIDAS analysis. Expression data generated from both the MIDAS and Acuity software were generally in agreement, thus supporting the reliability of the microarray results. Table 2 groups the transcripts that were significantly altered at 12 h post-infection according to their known functions, including mRNAs encoding four hypothetical proteins and eight ESTs with unknown roles.

Genes with altered transcriptional patterns belonged to a wide range of functional classes. For example, those involved in the host translational machinery, and mRNAs encoding structural proteins such as cytoskeleton-associated proteins were notably downregulated. In contrast, mRNAs of heat shock proteins (HSPs) were significantly elevated, a common phenomenon in cells experiencing external stresses or stimuli. However, transcripts of other functional categories exhibited variable responses to SARS-CoV infection.

3.2. Real-time RT-PCR analysis confirms modified transcription of specific genes

To verify the results of the microarray analysis of SARS-CoV-infected Vero E6 cells, real-time RT-PCR was performed for 17 interesting genes whose expression levels were either upregulated or downregulated. Only changes in relative expression levels greater than twofold were considered significant. With the HUEL gene serving as a normalization control, the changes in expression and the *P*-values are listed in Table 2. Our real-time analysis of HUEL gene expression also revealed that the difference in C_T between infected and uninfected samples was negligible (less than 0.5), thereby justifying the use of HUEL for normalization (data not shown). Overall, the gene expression trends by real-time RT-PCR concurred with the microarray data for all genes except one, although the magnitude of changes differed. The only discordant gene was MADH2, which mediates TGF-β signaling to regulate cell growth and differentiation. Expression of this transcript in infected cells increased by 4.65-fold by microarray analysis, but by only 1.6-fold via real-time RT-PCR. The differences in relative expression by these two techniques may be attributed to their differences in kinetics and sensitivity. In general, relative expression changes by real-time RT-PCR were greater than those by microarray analysis, especially for genes that were markedly overexpressed. This may be explained by the better sensitivity and reliability of real-time RT-PCR compared to microarray, whose drawback is the saturation of fluorescent signals.

The expression profiles in SARS-CoV-infected cells of additional genes absent from the microarray (DENN, FAIM, hIAP1 and Mx1) were also elucidated by real-time RT-PCR (Table 2). DENN, FAIM and hIAP1 participate in the anti-apoptotic mechanisms of host cells. Transcripts of DENN and hIAP1 were upregulated 3.75- and 3.54-fold, respectively, whereas FAIM was downregulated 5.46-fold. The mRNA of Mx1, an antiviral defense gene, was highly upregulated 59.51-fold. Real-time RT-PCR targeting a 182-bp fragment within the SARS-CoV RNA-dependent RNA polymerase gene provided an indication of the intensity of virus replication and viral load. Twelve hours after infection, we observed a 9.42×10^4-fold rise in SARS-CoV transcripts, corresponding to a C_T value of 5.6, reflecting the very rapid SARS-CoV replication process within Vero E6 cells.

3.3. The p53 splice variant is expressed in SARS-CoV-infected cells

A p53 gene fragment spanning exons 7–10, from both uninfected and infected Vero E6 cells, was amplified, the sequenc-

Table 2
Categories of human and viral genes displaying altered transcription profiles during SARS-CoV infection of Vero cells

GenBank accession no.	Gene	Fold change in transcription		
		Acuity	MIDAS	Real-time RT-PCR
Cell cycle and development				
NM_004417	Dual specificity phosphatase 1 (DUSP1)	19.15	11.12	42.67 (0.012)
NM_000136	Fanconi anemia, complementation group C (FANCC)	7.41	4.64	
NM_012206	Hepatitis A virus cellular receptor 1 (HAVCR1)	–11.11	–11.18	–10.27 (0.030)
NM_000598	Insulin-like growth factor binding protein 3 (IGFBP3)	–6.67	–8.72	–16.62 (0.001)
NM_005901	MAD, mothers against decapentaplegic homolog 2 (*Drosophila*) (MADH2)	5.71	4.65	1.60 (0.009)
NM_000582	Secreted phosphoprotein 1 (osteopontin, bone sialoprotein I, early T-lymphocyte activation 1) (SPP1)	–3.05	–5.88	
Cellular metabolism				
NM_001912	Cathepsin L (CTSL), transcript variant 1	–2.54	–4.36	–4.96 (0.017)
NM_000127	Exostoses (multiple) 1 (EXT1)	–2.86	–4.13	
NM_002410	Mannosyl (alpha-1,6-)-glycoprotein beta-1,6-N-acetyl-glucosaminyltransferase (MGAT5)	11.18	7.28	
Cytoskeleton-associated proteins				
NM_018477	Actin-related protein 10 homolog (*Saccharomyces cerevisiae*) (ACTR10)	–6.41	–8.62	
NM_003388	Cytoplasmic linker 2 (CYLN2)	–3.33	–4.50	
NM_015282	Cytoplasmic linker associated protein 1 (CLASP1)	–6.02	–7.17	
NM_021103	Thymosin, beta 10 (TMSB10)	–2.63	–4.09	
NM_021109	Thymosin, beta 4, X-linked (TMSB4X)	–4.44	–5.92	
DNA repair				
AY275681	MutS homolog 3 (*Escherichia coli*) (MSH3)	7.63	6.87	
Heat shock and stress response				
NM_006145	DnaJ (Hsp40) homolog, subfamily B, member 1 (DNAJB1)	11.02	8.56	
NM_006644	Heat shock 105/110 kDa protein 1 (HSPH1)	15.61	9.40	
NM_005345	Heat shock 70 kDa protein 1A (HSPA1A)	14.37	7.11	54.19 (0.002)
NM_005348	Heat shock 90-kDa protein 1, alpha (HSPCA)	7.00	4.06	7.09 (0.014)
mRNA processing factors				
NM_004593	Splicing factor, arginine/serine-rich 10 (transformer 2 homolog, *Drosophila*) (SFRS10)	4.38	5.09	
Protein modulators				
NM_004071	CDC-like kinase 1 (CLK1)	13.13	8.09	58.49 (0.005)
NM_007067	MYST histone acetyltransferase 2 (MYST2)	–4.22	–4.07	
NM_005742	Protein disulfide isomerase-related protein (P5)	–5.95	–5.80	
NM_002714	Protein phosphatase 1, regulatory subunit 10 (PPP1R10)	8.98	8.60	
NM_003255	Tissue inhibitor of metalloproteinase 2 (TIMP2)	–8.00	–9.69	–4.77 (0.012)
Signal transduction				
NM_004039	Annexin A2 (ANXA2)	–3.05	–4.39	–4.04 (0.009)
NM_000634	Interleukin 8 receptor, alpha (IL8RA)	4.44	4.47	26.91 (0.002)
NM_006860	RAB, member of RAS oncogene family-like 4 (RABL4)	9.91	8.99	
NM_006908	Ras-related C3 botulinum toxin substrate 1 (rho family, small GTP-binding protein Rac1) (RAC1)	–4.35	–4.43	–3.15 (0.020)
NM_001040	Sex hormone-binding globulin (SHBG)	5.80	5.77	
NM_003473	Signal transducing adaptor molecule 1 (STAM1)	6.56	4.29	13.74 (0.023)
Trafficking and protein degradation				
NM_014713	Lysosomal-associated protein transmembrane 4 alpha (LAPTM4A)	–4.59	–5.10	
NM_006432	Niemann-Pick disease, type C2 (NPC2)	–7.81	–8.93	–35.38 (0.013)
NM_003900	Sequestosome 1 (SQSTM1)	6.20	4.90	
Transcription and transcriptional regulators				
NM_000937	Polymerase (RNA) II (DNA directed) polypeptide A, 220 kDa (POLR2A)	9.24	6.18	
NM_181552	Cut-like 1, CCAAT displacement protein (*Drosophila*) (CUTL1)	–2.51	–4.54	
L17131	High-mobility group protein (HMG-I(Y)) gene	–38.46	–13.70	
NM_002158	Human T-cell leukemia virus enhancer factor (HTLF)	7.02	5.74	
NM_001730	Kruppel-like factor 5 (intestinal) (KLF5)	7.04	4.74	44.94 (0.001)
NM_005594	Nascent-polypeptide-associated complex alpha polypeptide (NACA)	–10.75	–10.75	
NM_020529	Nuclear factor of kappa light polypeptide gene enhancer in B-cells inhibitor, alpha (NFKBIA)	11.50	5.88	61.18 (0.008)

(continued on next page)

Table 2
(continued)

GenBank accession no.	Gene	Fold change in transcription		
		Acuity	MIDAS	Real-time RT-PCR
NM_003457	Zinc finger protein 207 (ZNF207)	–4.44	–4.48	
Translation				
NM_013417	Isoleucine-tRNA synthetase (IARS)	–8.13	–6.91	
NM_033251	Ribosomal protein L13 (RPL13)	–5.05	–7.16	
NM_000979	Ribosomal protein L18 (RPL18)	–4.35	–5.92	
NM_000980	Ribosomal protein L18a (RPL18A)	–7.94	–7.61	
NM_000990	Ribosomal protein L27a (RPL27A)	–4.59	–5.25	
NM_000967	Ribosomal protein L3 (RPL3)	–2.96	–5.23	
NM_033643	Ribosomal protein L36 (RPL36)	–8.55	–13.75	
NM_001014	Ribosomal protein S10 (RPS10)	–3.51	–4.56	
NM_001018	Ribosomal protein S15 (RPS15)	–4.23	–5.38	
NM_022551	Ribosomal protein S18 (RPS18)	–8.47	–8.59	
NM_001022	Ribosomal protein S19 (RPS19)	–7.81	–7.90	
NM_002952	Ribosomal protein S2 (RPS2)	–3.28	–4.76	
NM_001005	Ribosomal protein S3 (RPS3)	–2.39	–4.28	
NM_001402	Translation elongation factor 1 alpha 1 (EEF1A1)	–4.17	–5.77	
NM_001404	Translation elongation factor 1 gamma (EEF1G)	–3.60	–4.13	–4.13 (0.004)
NM_017646	tRNA isopentenyltransferase 1 (TRIT1)	–3.80	–4.38	
Hypothetical proteins				
BC047078	Hypothetical protein LOC283507	4.13	8.49	
NM_024511	Hypothetical protein MGC4701	5.54	5.03	
BC040148	Hypothetical protein MGC49942	–3.48	–4.46	
D63478	KIAA0144 gene	–4.74	–4.80	
Expressed sequence tags				
AK123640	cDNA FLJ41646 fis, clone FEBRA2024019	5.74	4.41	
AA968926	Op38b10.s1	10.41	10.75	
AI379149	Tc66a01.x1	–4.33	–5.40	
R60834	Yh04d12.r1	7.72	7.50	
N94144	Za25b09.r1	7.21	7.41	
W91949	Zh47e08.r1	6.36	6.86	
AA677283	Zj61d05.s1	–4.88	–4.76	
AA476783	Zw94h11.s1	2.88	6.93	
Additional genes				
U44953	DENN mRNA	N.A.	N.A.	3.75 (0.017)
NM_018147	Fas apoptotic inhibitory molecule (FAIM)	N.A.	N.A.	–5.46 (0.013)
AF070674	Inhibitor of apoptosis protein-1 (hIAP1)	N.A.	N.A.	3.54 (0.010)
NM_002462	Myxovirus (influenza virus) resistance 1, interferon-inducible protein p78 (mouse) (Mx1)	N.A.	N.A.	59.51 (0.004)
AY268070	SARS coronavirus RNA-directed RNA polymerase	N.A.	N.A.	9.42×10^4 (0.009)

The microarray data were analyzed using both Acuity and MIDAS software. For the real-time RT-PCR data, the values in brackets indicate the *P*-values at the 95% confidence level. The test of significance was performed based on the differences between duplicate values as well as between data for infected versus uninfected samples. N.A., not applicable.

ing of which corresponded to nucleotides 779–1131 of the wild-type African green monkey p53 gene (GenBank accession no. X16384). Intriguingly, an additional larger fragment (Fig. 1) from SARS-CoV-infected Vero E6 cells was also amplified, sequencing of which revealed that it spanned nucleotides 779–1095 and 1096–1131 of the p53 gene. Sequence analysis confirmed that this fragment contained an insertion of 133 nucleotides from intron 9, as previously reported in the MOLT-4 human acute lymphoblastic leukemia cell line [23]. Within this insertion is a premature termination codon upstream of exon 10, which is thus predicted to generate a truncated p53 product lacking the C-terminal amino acids encoded by exons 10 and 11. Compared with the genomic sequence of human p53 gene (GenBank accession no. X54156), the sequence of the 133-nucleotide insertion detected in infected Vero E6 cells harbored two point mutations, three base insertions and an 8-bp deletion, corresponding to that identified in MOLT-4 cells [23].

4. Discussion

Fever, dry cough, dyspnea, myalgia and lymphopenia are common characteristic clinical features of SARS patients [2,25,26], although these are also symptomatic of other respiratory infections. Chest radiographs of severely ill patients display rapid progression of unilateral peripheral air-space consolidation to bilateral patchy consolidation usually within

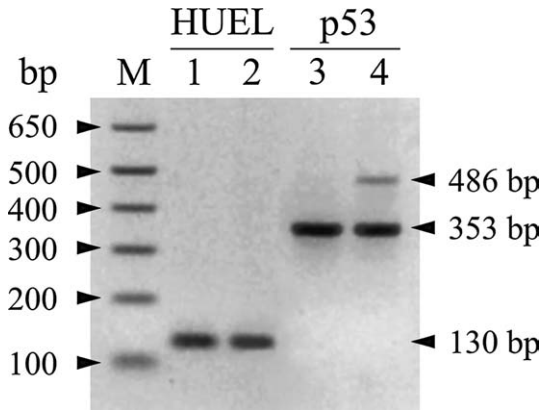

Fig. 1. RT-PCR analysis of p53 transcript variants. Lane M shows the DNA ladder markers. A 130-bp target fragment of the HUEL housekeeping gene transcript served as a normalization control to ensure equal amounts of starting cDNA template in uninfected (lane 1) and SARS-CoV-infected (lane 2) samples. The wild-type p53 gene was amplified as a 353-bp fragment in both uninfected (lane 3) and SARS-CoV-infected (lane 4) Vero E6 RNAs. However, an additional 486-bp fragment was amplified only from infected cells (lane 4), sequencing of which revealed its identity as the C-terminal alternatively spliced p53 transcript.

a week [27]. How this novel human CoV causes such extensive damage compared with other known human CoVs that are common etiologic agents of relatively mild upper respiratory illness remains to be fully elucidated. Interestingly, animal CoVs generally cause more severe diseases, and the civet cat is currently the prime suspect as the animal source of SARS-CoV that may have crossed the species barrier to humans. Examples of animal viruses crossing over to humans already exist, e.g. Nipah virus (pigs) and H5N1 influenza virus (poultry).

In order to understand the pathophysiology of SARS-CoV infection and host cellular responses, we employed cDNA microarray, RT-PCR and cDNA sequencing analyses to investigate the gene expression changes during the infection process. Similar studies have previously been conducted on infections with dengue virus [28], human polyomavirus JC [29] and herpes simplex virus [14]. Vero E6 served as the host cells for infection, as this cell line is the most permissive for SARS-CoV replication [1–3]. So far, human cell lines are not suitable, with the recent exception of LoVo cells, which are susceptible to SARS-CoV infection [30]. However, persistent infection occurs in LoVo cells with no visible CPE, in contrast to the lytic infection seen in Vero E6 cells which mimics the apoptosis observed in the respiratory epithelial cells of severely ill SARS patients [31–33]. The infection process is very rapid, such that virus particles are internalized into vacuoles within 10 min post-infection [34], extracellular virus particles exist in ~30% of the cells by 6 h post-infection, and numerous large vacuoles containing mature virus are present in the cytoplasm of infected cells from 12 to 21 h post-infection [13], as evident from the almost 10^5-fold increase in the level of SARS-CoV transcripts by real-time RT-PCR analysis. Expression of the novel SARS-CoV protein 3a is detectable in infected Vero E6 cells at 8–12 h post-infection, and also in the pneumocytes of a SARS patient's lung [35]. Furthermore, the incubation period of SARS is variously reported to be 6.4 days [36] or 5 days [37], with a range of 3–8 days [38]. Therefore, 12 h after infection of Vero cells represents an appropriate time-point that allows for a larger population of cells to be infected so that significant changes representative of the pathophysiological process of SARS-CoV infection can be elucidated. It would be ideal to conduct time–course experiments commencing from earlier time-points in the virus replication cycle.

Vero E6 cells are derived from African green monkey, and the limitations of cross hybridization may affect our microarray results. It is estimated that 95% of nucleotides are exactly shared between human and chimpanzee DNA [39]. Thus, the closest relative of humans is the chimpanzee, followed by the gorilla, orangutan and Old World monkeys (macaque and African green monkey), in increasing order of evolutionary divergence [40,41]. In view of the relatively small differences between the genomes of humans and primates [42], with most disparities arising from insertions, deletions and rearrangements [43], Vero cells represent a viable alternative model for investigating cellular gene responses to SARS-CoV in lieu of a human cell line. This was further substantiated by sequencing of the genes selected for real-time analyses, which revealed sequence differences of only 1–5% (data not shown).

From the microarray analysis, we identified 70 transcripts with altered expression that were classified according to their functional roles. The most distinguishable genes to be down-regulated by the infection were those involved in the host translational machinery, including 40S ribosomal proteins (RPS2, RPS3, RPS10, RPS15, RPS18, RPS19); 60S ribosomal proteins (RPL3, RPL13, RPL18, RPL18A, RPL27A, RPL36); isoleucine tRNA synthetase (IARS) and modifying enzyme (TRIT1); and eukaryotic translation elongation factors (EEF1A1 and EEF1G). Such host translational shutoff is frequently observed, as evident in infections with herpes simplex virus [44], influenza virus type A [45] and poliovirus [46]. However, unlike poliovirus infection, which often results in selective translation of viral uncapped mRNAs, CoVs give rise to mRNAs that are structurally similar to their eukaryotic hosts. This allows CoVs to parasitize upon the host machinery to translate the viral mRNA. Another study also indicates that murine CoV at high MOI inhibits host protein synthesis during the very early stage of infection, and suggests that the increased number of viral mRNAs produced during the later phase of infection compete with cellular mRNAs for cellular ribosomes [47].

SARS-CoV-infected cells also exhibited diminished expression of genes related to the maintenance of cytoskeletal structure. CYLN2 is associated with Williams syndrome, a multisystem developmental disorder [48]. It mediates the interaction between specific membranous organelles and microtubules, and may be an anti-catastrophic factor [49]. CLASP1 binds CYLN proteins and microtubules, colocalizing at the distal ends to provide stabilizing effects on the microtubules [50]. The microtubule network plays an important role in viral replication and viral protein trafficking [51].

Thus, disrupting the network may initially result in less virus production until a point at which the cells are overwhelmed by virus multiplication and then lyse to release virus particles. By exposing peritoneal macrophages to cytochalasin B, murine CoV infection changes from an acute cytopathology to a persistent type [52]. In SARS-CoV infection, these microtubule networks may become disrupted, making it conducive for persistent viral infection and subsequent release. Besides microtubules, the actin assembly may also be greatly affected by downregulation of TMSB4X and TMSB10, which are actin-sequestering proteins. Indeed, actin mRNAs are reduced in murine CoV infection [47]. Furthermore, reduction of TMSB4X transcripts may disrupt cellular functions, since TMSB4X may have a unique integrative function that links the actin cytoskeleton to important immune and cell growth-signaling cascades [53].

The upregulation of several HSPs was not unexpected given that elevation of HSP expression represents a crucial response towards external stimuli or stresses such as infections. Noteworthy is the strong induction of HSPA1A which is widely involved in translocation of membrane proteins, and acts as a scavenger of degraded peptides for antigen presentation. During a viral infection, a rise in the level of secreted cytokines such as interleukin 2 (IL-2) is often encountered. Besides inducing the proliferation of T lymphocytes, IL-2 also induces the expression of HSPA1A and HSPCA [54]. In certain inflammatory lung diseases with marked accumulation of eosinophils in the bronchoalveolar lavage, free oxygen radicals are produced which induce alveolar macrophages to synthesize antioxidants such as HSPs [55]. Such a phenomenon may operate in the atypical pneumonia characteristic of SARS patients who show significantly elevated plasma levels of IFN-gamma, IL-1, IL-6 and IL-12, IL-8, monocyte chemoattractant protein-1, and IFN-gamma-inducible protein-10 [56].

In our study, elevated expression of MGAT5 may contribute to the initiation of GlcNAc beta1,6 branching on *N*-glycans, thereby increasing *N*-acetyllactosamine, the ligand for galectins. In turn, galectins modulate T-cell proliferation as well as enhancing apoptosis at the site of antigen presentation [57]. Cathepsin L (CTSL) is a lysosomal cysteine proteinase that plays a major role in intracellular protein catabolism. Suppression of CTSL expression in A549 lung cancer cells leads to growth inhibition, which is compatible with CTSL downregulation during SARS-CoV infection. However, this growth inhibition is partially compensated by upregulation of IL-8 production [58]. In addition, CTSL secreted from human fibroblasts in response to external stimuli plays an important role in the processing of IL-8 to mature form in inflammatory sites [59].

Altered transcription of signal transduction molecules was also observed in SARS-CoV-infected cells. ANXA2, a fibrinolytic receptor, binds plasminogen and tissue plasminogen activator (t-PA) independently at the cell surface of monocytes and macrophages, thereby enhancing the catalytic efficiency of plasmin production [60], and limiting pulmonary fibrosis. However, the downregulation of ANXA2 in SARS-CoV infection is expected to decrease fibrinolysis. IL-8 is a member of the family of pro-inflammatory cytokines with roles in chemotaxis and activation of monocytes, selective chemotaxis of memory T cells, and induction of neutrophil infiltration in vivo. In dengue virus infection, IL-8 transcription is controlled by NFκB [61], which activates many immunoregulatory genes in response to pro-inflammatory stimuli. In our analysis, the upregulation of IL8RA (a low-affinity receptor for IL-8) implies more active IL-8 signal transduction at the site of inflammation, where the relative concentration of IL-8 is high [62].

The STAM1 protein contains an SH3 domain and an immunoreceptor tyrosine-based activation motif (ITAM). STAM1 associates with JAK3 and JAK2 kinases via its ITAM region, is phosphorylated by the JAK kinases upon cytokine stimulation, thus acting as an adaptor molecule involved in the downstream signaling of cytokine receptors [63]. STAM1 upregulation in our study suggests its enhanced role in the downstream signaling of cytokine receptors during SARS-CoV infection. In our model, several transcriptional modulators with altered expression may be crucial to the pathogenic outcome of infection.

The TIMP gene family encodes natural inhibitors of matrix metalloproteinases (a group of peptidases involved in degradation of the extracellular matrix) that regulate tumor growth, progression, and angiogenesis. TIMP2 activates Ras through a PKA-mediated pathway, leading to the formation of the Ras/PI3K complex, with roles in proliferation, differentiation, membrane ruffling, and prevention of apoptosis [64]. Reduced TIMP2 expression in SARS-CoV infection is thus predicted to promote apoptosis of infected cells.

Certain transcripts involved in cell cycle and development (e.g. DUSP1 and FANCC) were upregulated. DUSP1 plays an important role as a protein phosphatase in human cellular response to environmental stress, and as a negative regulator of cellular proliferation by inactivating mitogen-activated protein kinases (MAPK) [65]. IGFBP3 is essential for TNFα-induced apoptosis [66], but downregulation of its transcript level in SARS-CoV-infected cells may imply a mechanism to avert virus-induced apoptosis, thus favoring viral replication.

We also analyzed the transcriptional profiles of several apoptosis-related genes. SARS-CoV-infected Vero E6 cells exhibited upregulation of the combined transcripts of the anti-apoptotic DENN isoform and the pro-apoptotic IG20 isoform that both interact with tumor necrosis factor receptor 1 and participate in the MAPK pathway [67,68]. Increased transcript level of the hIAP1 apoptotic inhibitor [69] during SARS-CoV infection mirrored that observed in dengue virus infection of human umbilical vein endothelial cells [28]. Although infected Vero cells eventually lyse at the late phase of infection, hIAP1 may attenuate apoptosis at the early infection phase, thereby allowing the virus to replicate to high titer. In contrast, another anti-apoptotic gene, FAIM, was downregulated in SARS-CoV infection. The susceptibility of primary B cells to Fas-mediated apoptosis is modulated by FAIM

[70] and NFκB [71,72]. Thus, the lower expression of FAIM and the higher expression of NFKBIA which inhibits NFκB are likely to favor Fas-mediated apoptosis. In SARS-CoV infection, the elevated expression of NFKBIA, an inhibitor of the NFκB complex, may attenuate the effect of NFκB [73]. A critical regulator of apoptosis, NFκB is most commonly involved in the suppression of programmed cell death via the transactivation of anti-apoptotic gene expression [74]. NFκB also plays a key role in controlling cell proliferation, as evidenced by the deregulated expression of its constitutively active form in certain cancers such as Hodgkin's disease [75,76]. The interplay between, and altered expression of, apoptosis-related genes in SARS-CoV infection may help to achieve viral replication before cell death.

Mx proteins comprise a group of antiviral GTPases that play an important role in IFN-induced antiviral defenses [77]. They also act to sequester viral nucleocapsids and limit their accessibility for viral replication [78]. The marked elevation of Mx1 expression (~60-fold increase) at 12 h post-infection suggests a highly notable antiviral response to SARS-CoV pathogenesis.

In SARS-CoV-infected Vero cells, an additional larger transcript of the p53 tumor suppressor gene was detected, arising from the use of an alternative 5′ donor splicing site, with the resultant loss and modification of the C-terminus [23]. Various alternatively spliced p53 isoforms are expressed at relatively low levels and tend to be restricted to particular cell types and/or physiologic conditions [79]. The p53 C-terminus plays a pivotal role in regulating the activity of the wild-type molecule. Compared to the regularly spliced form of p53, the C-terminally altered p53 protein inhibits both p53-dependent apoptosis and transactivation [80]; binds more efficiently to DNA in a sequence-specific manner; is more efficient in concentration-dependent transcriptional repression of the promoter of the p21 cyclin-dependent kinase inhibitor gene; associates with and interferes more efficiently with binding of TATA-binding protein to a TATA-containing DNA sequence [81]. The presence of this p53 isoform with a truncated C-terminus is therefore expected to modify the activity of the wild-type p53, and exert a role in the pathogenesis of SARS-CoV infection.

Our study offers an overview of the cascade of changes in host cellular expression culminating from infection with SARS-CoV. The counterbalancing of several anti-inflammatory and pro-inflammatory pathways together with the variable expression of apoptosis-related genes was striking and instructive [82]. These molecular events underlie the mechanism that ensures cell survival during the early phase of infection to allow rapid multiplication of progeny virus before the CPE occur. Being deficient in IFN response, Vero cells may not necessarily represent physiologically normal cells. Nonetheless, alterations in transcription of genes that are conserved between African green monkeys and humans provide a better understanding of the biology of SARS-CoV infection. Such molecular insights into the pathophysiological mechanisms may lead to novel and viable strategies for intervention in the infection process [83].

Acknowledgments

The authors thank Takara Bio for providing the microarray slides, K.F. Tang and Judith Mah for assistance. This work was funded by a grant from the Biomedical Research Council, Singapore. W.F. Leong is the recipient of a Research Scholarship from the National University of Singapore.

References

[1] C. Drosten, S. Gunther, W. Preiser, S. Van der Werf, H.R. Brodt, S. Becker, H. Rabenau, M. Panning, L. Kolesnikova, R.A. Fouchier, A. Berger, A.M. Burguiere, J. Cinatl, M. Eickmann, N. Escriou, K. Grywna, S. Kramme, J.C. Manuguerra, S. Muller, V. Rickerts, M. Sturmer, S. Vieth, H.D. Klenk, A.D. Osterhaus, H. Schmitz, H.W. Doerr, Identification of a novel coronavirus in patients with severe acute respiratory syndrome, New Engl. J. Med. 348 (2003) 1967–1976.

[2] J.S. Peiris, S.T. Lai, L.L. Poon, Y. Guan, L.Y. Yam, W. Lim, J. Nicholls, W.K. Yee, W.W. Yan, M.T. Cheung, V.C. Cheng, K.H. Chan, D.N. Tsang, R.W. Yung, T.K. Ng, K.Y. Yuen, Coronavirus as a possible cause of severe acute respiratory syndrome, Lancet 361 (2003) 1319–1325.

[3] T.G. Ksiazek, D. Erdman, C.S. Goldsmith, S.R. Zaki, T. Peret, S. Emery, S. Tong, C. Urbani, J.A. Comer, W. Lim, P.E. Rollin, S.F. Dowell, A.E. Ling, C.D. Humphrey, W.J. Shieh, J. Guarner, C.D. Paddock, P. Rota, B. Fields, J. DeRisi, J.Y. Yang, N. Cox, J.M. Hughes, J.W. LeDuc, W.J. Bellini, L.J. Anderson, A novel coronavirus associated with severe acute respiratory syndrome, New Engl. J. Med. 348 (2003) 1953–1966.

[4] M. Surjit, B. Liu, P. Kumar, V.T.K. Chow, S.K. Lal, The nucleocapsid protein of the SARS coronavirus is capable of self-association through a C-terminal 209 amino acid interaction domain, Biochem. Biophys. Res. Commun. 317 (2004) 1030–1036.

[5] W. Ying, Y. Hao, Y. Zhang, W. Peng, E. Qin, Y. Cai, K. Wei, J. Wang, G. Chang, W. Sun, S. Dai, X. Li, Y. Zhu, J. Li, S. Wu, L. Guo, J. Dai, J. Wang, P. Wan, T. Chen, C. Du, D. Li, J. Wan, X. Kuai, W. Li, R. Shi, H. Wei, C. Cao, M. Yu, H. Liu, F. Dong, D. Wang, X. Zhang, X. Qian, Q. Zhuhai, F. He, Proteomic analysis on structural proteins of severe acute respiratory syndrome coronavirus, Proteomics 4 (2004) 492–504.

[6] H. Sun, H. Luo, C. Yu, T. Sun, J. Chen, S. Peng, J. Qin, J. Shen, Y. Yang, Y. Xie, K. Chen, Y. Wang, X. Shen, H. Jiang, Molecular cloning, expression, purification, and mass spectrometric characterization of 3C-like protease of SARS coronavirus, Protein Expr. Purif. 32 (2003) 302–308.

[7] G. Sutton, E. Fry, L. Carter, S. Sainsbury, T. Walter, J. Nettleship, N. Berrow, R. Owens, R. Gilbert, A. Davidson, S. Siddell, L.L. Poon, J. Diprose, D. Alderton, M. Walsh, J.M. Grimes, D.I. Stuart, The nsp9 replicase protein of SARS-coronavirus, structure and functional insights, Structure 12 (2004) 341–353.

[8] W. Gao, A. Tamin, A. Soloff, L. D'Aiuto, E. Nwanegbo, P.D. Robbins, W.J. Bellini, S. Barratt-Boyes, A. Gambotto, Effects of a SARS-associated coronavirus vaccine in monkeys, Lancet 362 (2003) 1895–1896.

[9] Z.Y. Yang, W.P. Kong, Y. Huang, A. Roberts, B.R. Murphy, K. Subbarao, G.J. Nabel, A DNA vaccine induces SARS coronavirus neutralization and protective immunity in mice, Nature 428 (2004) 561–564.

[10] J. Sui, W. Li, A. Murakami, A. Tamin, L.J. Matthews, S.K. Wong, M.J. Moore, A. St Clair Tallarico, M. Olurinde, H. Choe, L.J. Anderson, W.J. Bellini, M. Farzan, W.A. Marasco, Potent neutralization of severe acute respiratory syndrome (SARS) coronavirus by a human mAb to S1 protein that blocks receptor association, Proc. Natl. Acad. Sci. USA 101 (2004) 2536–2541.

[11] W. Li, M.J. Moore, N. Vasilieva, J. Sui, S.K. Wong, M.A. Berne, M. Somasundaran, J.L. Sullivan, K. Luzuriaga, T.C. Greenough, H. Choe, M. Farzan, Angiotensin-converting enzyme 2 is a functional receptor for the SARS coronavirus, Nature 426 (2003) 450–454.

[12] P. Wang, J. Chen, A. Zheng, Y. Nie, X. Shi, W. Wang, G. Wang, M. Luo, H. Liu, L. Tan, X. Song, Z. Wang, X. Yin, X. Qu, X. Wang, T. Qing, M. Ding, H. Deng, Expression cloning of functional receptor used by SARS coronavirus, Biochem. Biophys. Res. Commun. 315 (2004) 439–444.

[13] M.L. Ng, S.H. Tan, E.E. See, E.E. Ooi, A.E. Ling, Proliferative growth of SARS coronavirus in Vero E6 cells, J. Gen. Virol. 84 (2003) 3291–3303.

[14] M.F. Kramer, W.J. Cook, F.P. Roth, J. Zhu, H. Holman, D.M. Knipe, D.M. Coen, Latent herpes simplex virus infection of sensory neurons alters neuronal gene expression, J. Virol. 77 (2003) 9533–9541.

[15] S. Munir, V. Kapur, Regulation of host cell transcriptional physiology by the avian pneumovirus provides key insights into host–pathogen interactions, J. Virol. 77 (2003) 4899–4910.

[16] K.H. Limesand, S. Higgs, L.D. Pearson, B.J. Beaty, Effect of mosquito salivary gland treatment on vesicular stomatitis New Jersey virus replication and interferon alpha/beta expression in vitro, J. Med. Entomol. 40 (2003) 199–205.

[17] A.I. Saeed, V. Sharov, J. White, J. Li, W. Liang, N. Bhagabati, J. Braisted, M. Klapa, T. Currier, M. Thiagarajan, A. Sturn, M. Snuffin, A. Rezantsev, D. Popov, A. Ryltsov, E. Kostukovich, I. Borisovsky, Z. Liu, A. Vinsavich, V. Trush, J. Quackenbush, TM4: a free, open-source system for microarray data management and analysis, Biotechniques 34 (2003) 374–378.

[18] J. Quackenbush, Microarray data normalization and transformation, Nat. Genet. 32 (2002) 496–501.

[19] D.L.C. Sim, V.T.K. Chow, The novel human HUEL (C4orf1) gene maps to chromosome 4p12–p13 and encodes a nuclear protein containing the nuclear receptor interaction motif, Genomics 59 (1999) 224–233.

[20] D.L.C. Sim, W.M. Yeo, V.T.K. Chow, The novel human HUEL (C4orf1) protein shares homology with the DNA-binding domain of the XPA DNA repair protein and displays nuclear translocation in a cell cycle-dependent manner, Int. J. Biochem. Cell Biol. 34 (2002) 487–504.

[21] P.W.F. Leong, K. Liew, W. Lim, V.T.K. Chow, Differential display RT-PCR analysis of enterovirus-71-infected rhabdomyosarcoma cells reveals mRNA expression responses of multiple human genes with known and novel functions, Virology 295 (2002) 147–159.

[22] K.J. Liew, V.T.K. Chow, Differential display RT-PCR analysis of ECV304 endothelial-like cells infected with dengue virus type 2 reveals messenger RNA expression profiles of multiple human genes involved in known and novel roles, J. Med. Virol. 72 (2004) 597–609.

[23] V.T.K. Chow, H.H. Quek, E.P.C. Tock, Alternative splicing of the p53 tumor suppressor gene in the Molt-4 T-lymphoblastic leukemia cell line, Cancer Lett. 73 (1993) 141–148.

[24] Y.H. Yang, S. Dudoit, P. Luu, D.M. Lin, V. Peng, J. Ngai, T.P. Speed, Normalization for cDNA microarray data: a robust composite method addressing single and multiple slide systematic variation, Nucleic Acids Res. 30 (2002) e15.

[25] K.W. Tsang, P.L. Ho, G.C. Ooi, W.K. Yee, T. Wang, M. Chan-Yeung, W.K. Lam, W.H. Seto, L.Y. Yam, T.M. Cheung, P.C. Wong, B. Lam, M.S. Ip, J. Chan, K.Y. Yuen, K.N. Lai, A cluster of cases of severe acute respiratory syndrome in Hong Kong, N. Engl. J. Med. 348 (2003) 1977–1985.

[26] Z. Zhao, F. Zhang, M. Xu, K. Huang, W. Zhong, W. Cai, Z. Yin, S. Huang, Z. Deng, M. Wei, J. Xiong, P.M. Hawkey, Description and clinical treatment of an early outbreak of severe acute respiratory syndrome (SARS) in Guangzhou, PR China, J. Med. Microbiol. 52 (2003) 715–720.

[27] N. Lee, D. Hui, A. Wu, P. Chan, P. Cameron, G.M. Joynt, A. Ahuja, M.Y. Yung, C.B. Leung, K.F. To, S.F. Lui, C.C. Szeto, S. Chung, J.J. Sung, A major outbreak of severe acute respiratory syndrome in Hong Kong, N. Engl. J. Med. 348 (2003) 1986–1994.

[28] R.V. Warke, K. Xhaja, K.J. Martin, M.F. Fournier, S.K. Shaw, N. Brizuela, N. De Bosch, D. Lapointe, F.A. Ennis, A.L. Rothman, I. Bosch, Dengue virus induces novel changes in gene expression of human umbilical vein endothelial cells, J. Virol. 77 (2003) 11822–11832.

[29] S. Radhakrishnan, J. Otte, S. Enam, L. Del Valle, K. Khalili, J. Gordon, JC virus-induced changes in cellular gene expression in primary human astrocytes, J. Virol. 77 (2003) 10638–10644.

[30] P.K. Chan, K.F. To, A.W. Lo, J.L. Cheung, I. Chu, F.W. Au, J.H. Tong, J.S. Tam, J.J. Sung, H.K. Ng, Persistent infection of SARS coronavirus in colonic cells in vitro, J. Med. Virol. 74 (2004) 1–7.

[31] H. Yan, G. Xiao, J. Zhang, Y. Hu, F. Yuan, D.K. Cole, C. Zheng, G.F. Gao, SARS coronavirus induces apoptosis in Vero E6 cells, J. Med. Virol. 73 (2004) 323–331.

[32] Z.W. Lang, L.J. Zhang, S.J. Zhang, X. Meng, J.Q. Li, C.Z. Song, L. Sun, Y.S. Zhou, D.E. Dwyer, A clinicopathological study of three cases of severe acute respiratory syndrome (SARS), Pathology 35 (2003) 526–531.

[33] G.M. Tse, K.F. To, P.K. Chan, A.W. Lo, K.C. Ng, A. Wu, N. Lee, H.C. Wong, S.M. Mak, K.F. Chan, D.S. Hui, J.J. Sung, H.K. Ng, Pulmonary pathological features in coronavirus associated severe acute respiratory syndrome (SARS), J. Clin. Pathol. 57 (2004) 260–265.

[34] M.L. Ng, S.H. Tan, E.E. See, E.E. Ooi, A.E. Ling, Early events of SARS coronavirus infection in vero cells, J. Med. Virol. 71 (2003) 323–331.

[35] C.J. Yu, Y.C. Chen, C.H. Hsiao, T.C. Kuo, S.C. Chang, C.Y. Lu, W.C. Wei, C.H. Lee, L.M. Huang, M.F. Chang, H.N. Ho, F.J. Lee, Identification of a novel protein 3a from severe acute respiratory syndrome coronavirus, FEBS Lett. 565 (2004) 111–116.

[36] C.A. Donnelly, A.C. Ghani, G.M. Leung, A.J. Hedley, C. Fraser, S. Riley, L.J. Abu-Raddad, L.M. Ho, T.Q. Thach, P. Chau, K.P. Chan, T.H. Lam, L.Y. Tse, T. Tsang, S.H. Liu, J.H. Kong, E.M. Lau, N.M. Ferguson, R.M. Anderson, Epidemiological determinants of spread of causal agent of severe acute respiratory syndrome in Hong Kong, Lancet 361 (2003) 1761–1766.

[37] M. Varia, S. Wilson, S. Sarwal, A. McGeer, E. Gournis, E. Galanis, B. Henry, Hospital Outbreak Investigation Team, Investigation of a nosocomial outbreak of severe acute respiratory syndrome (SARS) in Toronto, Canada, Can. Med. Assoc. J. 169 (2003) 285–292.

[38] K.Y. Chow, C.E. Lee, M.L. Ling, D.M. Heng, S.G. Yap, Outbreak of severe acute respiratory syndrome in a tertiary hospital in Singapore, linked to an index patient with atypical presentation: epidemiological study, BMJ 328 (2004) 195.

[39] R.J. Britten, Divergence between samples of chimpanzee and human DNA sequences is 5%, counting indels, Proc. Natl. Acad. Sci. USA 99 (2002) 13633–13635.

[40] J. Shi, H. Xi, Y. Wang, C. Zhang, Z. Jiang, K. Zhang, Y. Shen, L. Jin, K. Zhang, W. Yuan, Y. Wang, J. Lin, Q. Hua, F. Wang, S. Xu, S. Ren, S. Xu, G. Zhao, Z. Chen, L. Jin, W. Huang, Divergence of the genes on human chromosome 21 between human and other hominoids and variation of substitution rates among transcription units, Proc. Natl. Acad. Sci. USA 100 (2003) 8331–8336.

[41] M.J. Kelley, M. Pech, H.N. Seuanez, J.S. Rubin, S.J. O'Brien, S.A. Aaronson, Emergence of the keratinocyte growth factor multigene family during the great ape radiation, Proc. Natl. Acad. Sci. USA 89 (1992) 9287–9291.

[42] M.V. Olson, A. Varki, Sequencing the chimpanzee genome: insights into human evolution and disease, Nat. Rev. Genet. 4 (2003) 20–28.

[43] K.A. Frazer, X. Chen, D.A. Hinds, P.V. Pant, N. Patil, D.R. Cox, Genomic DNA insertions and deletions occur frequently between humans and nonhuman primates, Genome Res. 13 (2003) 341–346.

[44] D.N. Everly, P. Feng, I.S. Mian, G.S. Read, mRNA degradation by the virion host shutoff (Vhs) protein of herpes simplex virus: genetic and biochemical evidence that Vhs is a nuclease, J. Virol. 76 (2002) 8560–8571.

[45] M.S. Garfinkel, M.G. Katze, Translational control by influenza virus. Selective and cap-dependent translation of viral mRNAs in infected cells, J. Biol. Chem. 267 (1992) 9383–9390.

[46] N.M. Kuyumcu-Martinez, M.E. Van Eden, P. Younan, R.E. Lloyd, Cleavage of poly(A)-binding protein by poliovirus 3C protease inhibits host cell translation: a novel mechanism for host translation shutoff, Mol. Cell. Biol. 24 (2004) 1779–1790.

[47] A. Hilton, L. Mizzen, G. MacIntyre, S. Cheley, R. Anderson, Translational control in murine hepatitis virus infection, J. Gen. Virol. 67 (1986) 923–932.

[48] L.R. Osborne, D. Martindale, S.W. Scherer, X.M. Shi, J. Huizenga, H.H. Heng, T. Costa, B. Pober, L. Lew, J. Brinkman, J. Rommens, B. Koop, L.C. Tsui, Identification of genes from a 500-kb region at 7q11.23 that is commonly deleted in Williams syndrome patients, Genomics 36 (1996) 328–336.

[49] C.C. Hoogenraad, B.H. Eussen, A. Langeveld, R. Van Haperen, S. Winterberg, C.H. Wouters, F. Grosveld, C.I. De Zeeuw, N. Galjart, The murine CYLN2 gene: genomic organization, chromosome localization, and comparison to the human gene that is located within the 7q11.23 Williams syndrome critical region, Genomics 53 (1998) 348–358.

[50] A. Akhmanova, C.C. Hoogenraad, K. Drabek, T. Stepanova, B. Dortland, T. Verkerk, W. Vermeulen, B.M. Burgering, C.I. De Zeeuw, F. Grosveld, N. Galjart, Clasps are CLIP-115 and -170 associating proteins involved in the regional regulation of microtubule dynamics in motile fibroblasts, Cell 104 (2001) 923–935.

[51] J.M. Pasick, K. Kalicharran, S. Dales, Distribution and trafficking of JHM coronavirus structural proteins and virions in primary neurons and the OBL-21 neuronal cell line, J. Virol. 68 (1994) 2915–2928.

[52] L. Mallucci, B. Edwards, Influence of the cytoskeleton on the expression of a mouse hepatitis virus (MHV-3) in peritoneal macrophages: acute and persistent infection, J. Gen. Virol. 63 (1982) 217–221.

[53] M.R. Bubb, Thymosin beta 4 interactions, Vitam. Horm. 66 (2003) 297–316.

[54] D.K. Ferris, A. Harel-Bellan, R.I. Morimoto, W.J. Welch, W.L. Farrar, Mitogen and lymphokine stimulation of heat shock proteins in T lymphocytes, Proc. Natl. Acad. Sci. USA 85 (1988) 3850–3854.

[55] B.S. Polla, S. Kantengwa, G.J. Gleich, M. Kondo, C.M. Reimert, A.F. Junod, Spontaneous heat shock protein synthesis by alveolar macrophages in interstitial lung disease associated with phagocytosis of eosinophils, Eur. Respir. J. 6 (1993) 483–488.

[56] P.J. Openshaw, What does the peripheral blood tell you in SARS? Clin. Exp. Immunol. 136 (2004) 11–12.

[57] M. Demetriou, M. Granovsky, S. Quaggin, J.W. Dennis, Negative regulation of T-cell activation and autoimmunity by Mgat5 *N*-glycosylation, Nature 409 (2001) 733–739.

[58] A. Wille, A. Heimburg, A. Gerber, A. Reisenauer, T. Welte, F. Buhling, Functional consequences of cathepsin L deficiency in human lung epithelial cells, Biol. Chem. 383 (2002) 1291–1296.

[59] K. Ohashi, M. Naruto, T. Nakaki, E. Sano, Identification of interleukin-8 converting enzyme as cathepsin L, Biochim. Biophys. Acta 1649 (2003) 30–39.

[60] C. Brownstein, A.B. Deora, A.T. Jacovina, R. Weintraub, M. Gertler, K.M. Khan, D.J. Falcone, K.A. Hajjar, Annexin II mediates plasminogen-dependent matrix invasion by human monocytes: enhanced expression by macrophages, Blood 103 (2004) 317–324.

[61] I. Bosch, K. Xhaja, L. Estevez, G. Raines, H. Melichar, R.V. Warke, M.V. Fournier, F.A. Ennis, A.L. Rothman, Increased production of interleukin-8 in primary human monocytes and in human epithelial and endothelial cell lines after dengue virus challenge, J. Virol. 76 (2002) 5588–5597.

[62] A. Chuntharapai, K.J. Kim, Regulation of the expression of IL-8 receptor A/B by IL-8: possible functions of each receptor, J. Immunol. 155 (1995) 2587–2594.

[63] T. Takeshita, T. Arita, H. Asao, N. Tanaka, M. Higuchi, H. Kuroda, K. Kaneko, H. Munakata, Y. Endo, T. Fujita, K. Sugamura, Cloning of a novel signal-transducing adaptor molecule containing an SH3 domain and ITAM, Biochem. Biophys. Res. Commun. 225 (1996) 1035–1039.

[64] T. Wang, K. Yamashita, K. Iwata, T. Hayakawa, Both tissue inhibitors of metalloproteinases-1 (TIMP-1) and TIMP-2 activate Ras but through different pathways, Biochem. Biophys. Res. Commun. 296 (2002) 201–205.

[65] S.M. Keyse, E.A. Emslie, Oxidative stress and heat shock induce a human gene encoding a protein–tyrosine phosphatase, Nature 359 (1992) 644–647.

[66] R. Rajah, K.W. Lee, P. Cohen, Insulin-like growth factor binding protein-3 mediates tumor necrosis factor-alpha-induced apoptosis: role of Bcl-2 phosphorylation, Cell Growth Differ. 13 (2002) 163–171.

[67] K.M. Lim, V.T. Chow, Induction of marked apoptosis in mammalian cancer cell lines by antisense DNA treatment to abolish expression of DENN (differentially expressed in normal and neoplastic cells), Mol. Carcinog. 35 (2002) 110–126.

[68] K.M. Lim, W.S. Yeo, V.T. Chow, Antisense abrogation of DENN expression induces apoptosis of leukemia cells in vitro, causes tumor regression in vivo and alters the transcription of genes involved in apoptosis and the cell cycle, Int. J. Cancer 109 (2004) 24–37.

[69] P. Liston, S.S. Young, A.E. Mackenzie, R.G. Korneluk, Life and death decisions: the role of the IAPs in modulating programmed cell death, Apoptosis 2 (1997) 423–441.

[70] T.J. Schneider, G.M. Fischer, T.J. Donohoe, T.P. Colarusso, T.L. Rothstein, A novel gene coding for a Fas apoptosis inhibitory molecule (FAIM) isolated from inducibly Fas-resistant B lymphocytes, J. Exp. Med. 189 (1999) 949–956.

[71] T.L. Rothstein, X. Zhong, B.R. Schram, R.S. Negm, T.J. Donohoe, D.S. Cabral, L.C. Foote, T.J. Schneider, Receptor-specific regulation of B-cell susceptibility to Fas-mediated apoptosis and a novel Fas apoptosis inhibitory molecule, Immunol. Rev. 176 (2000) 116–133.

[72] B.R. Schram, T.L. Rothstein, NF-kappa B is required for surface Ig-induced Fas resistance in B cells, J. Immunol. 170 (2003) 3118–3124.

[73] N. Auphan, J.A. DiDonato, C. Rosette, A. Helmberg, M. Karin, Immunosuppression by glucocorticoids: inhibition of NF-kappa B activity through induction of I kappa B synthesis, Science 270 (1995) 286–290.

[74] J. Kucharczak, M.J. Simmons, Y. Fan, C. Gelinas, To be, or not to be: NF-kappaB is the answer—role of Rel/NF-kappaB in the regulation of apoptosis, Oncogene 22 (2003) 8961–8982.

[75] S.C. Sun, G. Xiao, Deregulation of NF-kappaB and its upstream kinases in cancer, Cancer Metastasis Rev. 22 (2003) 405–422.

[76] A. Younes, A. Garg, B.B. Aggarwal, Nuclear transcription factor-kappaB in Hodgkin's disease, Leuk. Lymphoma 44 (2003) 929–935.

[77] M.A. Horisberger, Interferon-induced human protein MxA is a GTPase which binds transiently to cellular proteins, J. Virol. 66 (1992) 4705–4709.

[78] G. Kochs, C. Janzen, H. Hohenberg, O. Haller, Antivirally active MxA protein sequesters La Crosse virus nucleocapsid protein into perinuclear complexes, Proc. Natl. Acad. Sci. USA 99 (2002) 3153–3158.

[79] S. Courtois, C.C. de Fromentel, P. Hainaut, p53 protein variants: structural and functional similarities with p63 and p73 isoforms, Oncogene 23 (2004) 631–638.

[80] N. Almog, N. Goldfinger, V. Rotter, p53-dependent apoptosis is regulated by a C-terminally alternatively spliced form of murine p53, Oncogene 19 (2000) 3395–3403.

[81] H. Huang, S. Kaku, C. Knights, B. Park, J. Clifford, M. Kulesz-Martin, Repression of transcription and interference with DNA binding of TATA-binding protein by C-terminal alternatively spliced p53, Exp. Cell Res. 279 (2002) 248–259.

[82] J.C. Reed, K.S. Doctor, A. Godzik, The domains of apoptosis: a genomics perspective, Sci. STKE 2004 (2004) re9.

[83] S.H. Huang, T. Triche, A.Y. Jong, Infectomics: genomics and proteomics of microbial infections, Funct. Integr. Genomics 1 (2002) 331–344.